Surface & Coatings Technology 407 (2021) 126764

Contents lists available at ScienceDirect

Surface & Coatings Technology

journal homepage: www.elsevier.com/locate/surfcoat

In-vitro cell interaction and apatite forming ability in simulated body fluid of ICIE16 and 13-93 bioactive glass coatings deposited by an emerging suspension high velocity oxy fuel (SHVOF) thermal spray

S. Bano [a], A. Rincon Romero [a], D.M. Grant [a], A. Nommeots-Nomm [b], C. Scotchford [a], I. Ahmed [a], T. Hussain [a,*]

[a] Faculty of Engineering, Advanced Materials Research Group, University of Nottingham, NG7 2RD, UK
[b] Imperial College London, Department of Materials, Royal School of Mines, Exhibition Road, London SW7 2AZ, UK

ARTICLE INFO

Keywords:
ICIE16
13-93
Bioactive glass
Simulated body fluid (SBF)
Hydroxyapatite (HA)
SHVOF
Cytotoxicity
MG63

ABSTRACT

ICIE16 and 13-93 bioactive glasses have been proposed as alternative chemically stable compositions in physiological fluid keeping bioactivity comparable to Bioglass®. ICIE16 and 13-93 bioactive glasses coatings were produced via an emerging suspension high-velocity oxy-fuel (SHVOF) thermal spraying technique. Suspensions of ICIE16 and 13-93 with 10 wt% solid loading in isopropanol (IPA) and water were used to produce coatings on AISI304 stainless steel using a flame power of 50 kW and 75 kW. For both glass formulations, the coatings deposited at a lower flame power were more porous, less hard, and less rough (~6% porous and 242 HV) than the coatings obtained at a higher flame power (~4% porosity and 300 HV). ICIE16 coatings showed more dissolution in SBF (simulated body fluid) than the 13-93 coatings. Moreover, the 13-93 glass coating sprayed at 75 kW showed the highest stability in SBF since only 2% of the coating was resorbed in SBF after 7 days of immersion and revealed apatite precipitation after 7 days. In-vitro cell tests, using MG63 cells, showed good cell attachment and proliferation on the surfaces of the coatings, revealing good cytocompatibility. The 13-93 coating sprayed at 75 kW revealed the highest cell proliferation after 7 days of incubation. This can be attributed to the higher surface roughness of the coating (Ra = 6.5 ± 0.6 μm).

1. Introduction

Several bioactive silicate-based glass formulations with excellent bone bonding properties in biomedical applications have been developed over the years [1]. The bioactivity of bioactive glasses has been attributed to the formation of hydroxyapatite (HA) layer on the surface, which was similar to the mineral component of human bone, and the rate of tissue formation was shown to be dependent on the rate of HA formation on the surface of implant. Three main processes lead to the formation of HA: ion exchange, dissolution, and precipitation [2,3]. Hench et al. [4] developed the first bioactive glass, Bioglass® (45S5), containing 45% SiO_2, 24.5% Na_2O, 24.5% CaO and 6% P_2O_5 (wt%), which forms a good bond with the bone at the interface between the implant and the host tissue and is suitable for rapid bone regeneration. The network connectivity (NC) for Bioglass® is 2.11, which is the mean number of bridging oxygens per silicon atom and is a predicator of the bioactivity and hence reactivity in the physiological fluid of the composition. Low NC means high dissolution rate and apatite forming ability in physiological fluid [5]. Due to high apatite forming ability and dissolution of Bioglass®, the coatings deposited with this glass may degrade over time and subsequently resulting in instability of the implant in the long term [6], therefore there is a need to explore coatings with new bioactive glass compositions that could survive for longer [7].

ICIE16 is a bioactive silicate glass that has composition closer to 45S5, with a NC of 2.13 that is higher than 45S5 due to a higher silica content [8,9]. The composition is 48% SiO_2, 33% CaO, 6.6% Na_2O, 2.4% P_2O_5 and 10% K_2O, in wt%. By adding a second alkali oxide such as K_2O to the glass composition, physical and chemical properties of bioactive glasses can be tailored; this is called 'mixed alkali effect (MAE)'. With this addition, the problem associated with the solubility of Bioglass® in physiological fluid can be overcome [10]. However, with the addition of K_2O, apatite forming ability was reduced [11].

Another alternative bioactive glass based on Bioglass® composition is 13-93, which was first investigated by Brink et al. [12]. This

* Corresponding author.
E-mail address: tanvir.hussain@nottingham.ac.uk (T. Hussain).

https://doi.org/10.1016/j.surfcoat.2020.126764
Received 12 October 2020; Received in revised form 27 November 2020; Accepted 10 December 2020
Available online 18 December 2020

Table 1
As prepared melt-quenched nominal compositions of glasses (in wt%).

(wt%)	SiO_2	CaO	Na_2O	K_2O	P_2O_5	MgO
ICIE16	48	33	6.6	10	2.4	–
13-93	53	20	6.0	12	4	5

composition has a comparatively higher silica content and additional network modifiers such as K_2O and MgO (53 wt% SiO_2, 6 wt% Na_2O, 20 wt% CaO, 12 wt% K_2O, 5 wt% MgO and 4 wt% P_2O_5) [11,13,14]. The NC of 13-93 bioactive glass is 2.58 due to the higher silica content [9]. In addition, the presence of MgO makes this glass less vulnerable to dissolution and hence yields a reduced apatite forming ability [16,17]. MgO is also a cofactor in several enzymes necessary for bone health [18]; as investigated by Ferreira et al., bioactive glasses incorporating MgO are suitable for osteoblast-like cell proliferation [19].

Thermal spraying of bioactive glasses offers the opportunity to coat metallic implants with tailored layers for biomedical applications. Additionally, bioactive glasses are suitable candidates to produce thermal sprayed coatings as they substantially preserve their original composition and structure in comparison to thermal sprayed coatings of bioactive ceramic or synthetic HA. Synthetic HA tends to partially decompose, during thermal spray, resulting in coatings with both amorphous and crystalline phases, leading to a bioactivity reduction [15]. Suspension high velocity oxy-fuel (SHVOF) thermal spraying is a coating deposition technique with the key advantage of enabling processing of nano and micrometric particles in a suspension [16–18]. This process relies upon a modified HVOF torch to spray a stable suspension instead of powder feedstock [19]. It has been shown that the use of a suspension as feedstock allows the production of nano structured coatings with improved strength and durability [17,18,20,21]. The process involves the direct injection of the suspension into the combustion chamber, which favours significant heat transfer between particles and the flame. After solvent evaporation, the particles are heated by the gas in the combustion chamber and expansion nozzle. When this gas attains supersonic velocity upon expansion to ambient pressure outside of the torch, the particles are ejected at high velocity towards the substrate. This process produces layers of flattened particles, resulting in a dense thick microstructure coating with high cohesive and adhesive strength [22]. This process has already been experimentally verified for bioactive coatings such as Bioglass® [23–25].

SHVOF has been shown to be an effective technique for the deposition of bioactive glass coatings. For instance, Altomare et al. [25] produced Bioglass® coatings using SHVOF thermal spray, revealing cytocompatibility towards MG63 cell. However, the coatings microstructures exhibited a gradient, so the process parameters need to be optimised to reduce the overall porosity. Other bioactive glass coatings have been deposited and proved to be bioactive as reported in the literature; however, it was found that the microstructure of these coatings depends on the process parameters [26–28]. Generally, SHVOF thermal spray can produce high quality dense bioactive glass coatings [22,24].

Here the production of ICIE16 and 13-93 bioactive glass coatings is reported for the first time, showing the significant flexibility of SHVOF to produce bioactive coatings. The main objective was to study and optimise the spray parameters in order to tailor the glass coating microstructure and obtain the best mechanical and bioactive properties. The second objective was to investigate in-vitro biological response to these coatings using MG-63 cells.

2. Experimental

2.1. Feedstock preparation and characterisation

Bioactive glasses ICIE16 and 13-93, with nominal compositions stated in Table 1, were produced from the appropriate masses of analytical grade reagents, silica (Prince Minerals, Stoke on Trent, UK), sodium carbonate, potassium carbonate, magnesium oxide, calcium carbonate and calcium phosphate (Sigma Aldrich Dorset, UK). The reagents were heated to 1400 °C for 2 h in a 95 wt% platinum 5 wt% gold crucible, and the melt was then quenched at room temperature, forming a coarse frit that was collected and dried at 100 °C.

Frits of ICIE16 and 13-93 were ground separately in a zirconia jar with zirconia balls of 5 mm diameter for 30 min and 550 rpm using PM-100 ball mill (Retsch1-5, Germany), which resulted in $D_{10} = 1.8$ μm, $D_{50} = 8.3$ μm and $D_{90} = 24$ μm for the ICIE16 powders and for 13-93 powders of $D_{10} = 1$ μm, $D_{50} = 4$ μm and $D_{90} = 20$ μm. In order to obtain finer powders for suspension preparation, the powders were again dry milled with 2 mm zirconia beads for 30 min at 500 rpm. In all cases of milling the weight ratio of balls to materials was kept at approximately 5.

Laser diffractometer (Beckman Coulter, Inc., 250 S. Kraemer Blvd. Brea, California 92,821, USA) with a 750 nm laser was used to measure particle size distribution (D_{10}, D_{50}, and D_{90}). For both of the glasses the powder samples were examined with SEM (JEOL 6490, Tokyo, Japan) at a working distance of 10 mm and accelerating voltage of 20 kV, in secondary electron mode (SE) for powder morphology, and energy dispersive x-rays spectroscopy (EDX) analysis (INCA 350, Oxford Instruments, Abingdon, UK).

Table 2
Process parameters for SHVOF spray of ICIE16 and 13-93 bioactive glass coatings.

Run. number	H_2 flow rate (slpm)	O_2 flow rate (slpm)	Torch passes	Flame heat power (kW)
R50	355	152	20	50
R75	527	226	20	75

2.2. Spray process

Suspensions of ICIE16 and 13-93 powders were prepared to a 10 wt% solid loading, using a mixture of water and 15 wt% isopropyl alcohol (IPA) (VWR chemicals, UK) as suspending media. These suspensions were directly injected at the centre of the gas mixing block of a modified TopGun HVOF thermal spray unit (GTV GmbH, Germany) with a combustion chamber with a length of 22 mm, a barrel nozzle of 110 mm, and a diameter of 0.3 mm. The suspension was fed at 50 ml/min flow rate from a 2 l vessel at a pressure of 3 bar. During spray, the suspension was continuously stirred to prevent sedimentation and agglomeration. Additional process parameters, i.e. fuel gas (hydrogen) and oxygen flow rates, optimised in a previous work [7], are given in Table 2.

AISI304 stainless steel substrates (nominal composition of 19.0 Cr, 9.2 Ni, 1.0 Si, 2.0 Mn, 0.04 P, 0.08 C, 0.03 S and 68.6 Fe—all in wt%) (60 × 25 × 2 mm) were used in this study. Before coating deposition, the substrates were grit blasted (Guyson blast cleaner, England) using F100 brown alumina with a size range from 0.125 to 0.149 mm at pressure of 3 bar. Substrates were then cleaned in an ultrasonic bath using industrial methylated spirit for 10 min and were mounted onto a rotating carousel (at 73 rpm) of twelve substrates. The spray gun was scanned vertically up and down at a speed of 5 mm/s to deposit a coating of the desired thickness. The stand-off distance was set to 85 mm for all runs, which underwent 20 passes, and during and after every run compressed air jet was directed to the carousel for cooling purposes.

2.3. Coating characterisation

Coated samples were cut transversely with a SiC cutting wheel (MetPrep Ltd, Coventry, United Kingdom) at a speed of 0.025 mm/s using precision cutting machine (Brilliant 220, ATM GmbH, Mammelzen, Germany), cold mounted in conductive resin (Epoxy resin, Startus ApS, Denmark), then ground and polished to a 1 μm diamond finish and

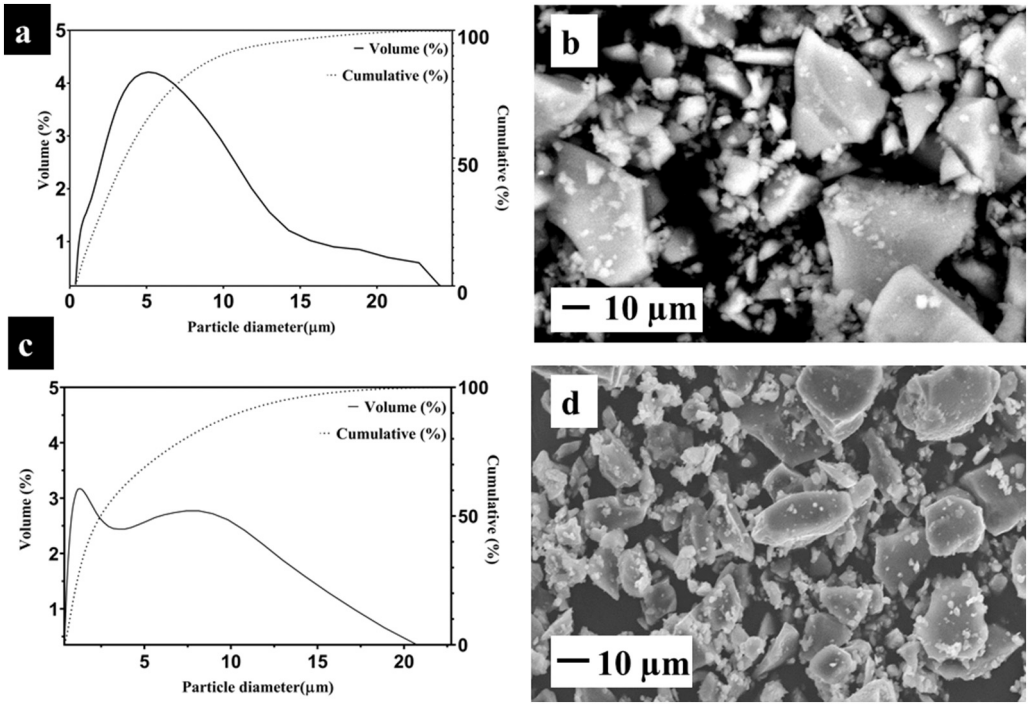

Fig. 1. Particle size distribution (a) SEM image (b) of ICIE16, particle size distribution (c) and SEM image (d) of 13-93 bioactive glass.

then carbon coated for SEM examination.

The polished cross sections and the surfaces of the coatings were observed with SEM (JEOL 6490, Tokyo, Japan) at 20 kV with 10 mm working distance in SE imaging mode. INCA software (INCA 350, Oxford Instruments, Abingdon, UK) was used for EDX analysis acquired in different points across a perpendicular line though the coating cross section and different areas on the surface of the coatings.

Surface roughness (R_a) of the coatings was measured using Talysurf Profilometer (Taylor Hobson Ltd, UK) with stylus radius 2 μm, sampling distance of 0.5 μm in the scan direction while speed of stylus was 0.25 mm/s.

The porosity of each coating was analysed by ImageJ (NIH, USA) software with thresholding technique to highlight features of interest with five SEM SE images of 1000× magnification from different regions of the cross section (172 × 156 μm). Coating thickness was measured with the same software on SE SEM images. Microhardness measurements were done on the polished cross section of the coatings with a Vickers microhardness tester (BUEHLER, UK) employing 25 gf load for 30 s dwell time by making 5 indents.

ICIE16 and 13-93 bioactive glass coatings and powders were also investigated via X-ray diffraction to explore if any phase changes had occurred, pre- and post-processing. An XRD (D500 Siemens with a Cu K_α radiation source $\lambda = 1.54$ Å), was utilised scanning over a 2θ range from 20° to 70°, with a step size of 0.05° and a dwell time of 7 s. Raman spectroscopy was also performed using a LabRAM HR spectrometer (HORIBA Jobin Yvon, Japan). Spectra were acquired using a 532 nm laser, a 100× objective, 300 μm confocal pinhole and 600 lines/mm diffracting grating. Spectra were recorded for 15 s and 20 accumulations on the surface of the coatings.

2.4. In vitro simulated body fluid (SBF) tests

Immersion tests in simulated body fluid (SBF) were performed using samples of 10 mm × 10 mm, cut from coated samples with the abrasive cutting machine (AbrasiMatic 300, Bueher. UK). SBF was prepared using the detailed procedure described in BS ISO 23317:2014 [29]. The immersion tests were carried out in closed plastic containers in a specific volume of (Vs) of SBF, such that Vs = Sa/10 (where Sa is the surface area of samples (100 mm^2) considering that the square samples have a side of 10 mm) at a constant temperature of 37 °C, and the samples were immersed for 1, 3 and 7 days. After extraction from the SBF, samples were washed with double distilled water and dried at room temperature.

The samples were then characterised for any morphological and compositional changes. Sample surfaces were investigated with SEM JEOL 6490 for SE and back scattered electrons (BSE) imaging and EDX analysis. XRD and Raman were also performed on these samples to identify any HA deposited on the samples after SBF tests.

2.5. In vitro cell interaction

Cytocompatibility tests of ICIE16 and 13-93 coatings were performed using osteosarcoma cell line MG63. Samples were cut in 10 mm diameter discs using water jet cutting machine. These samples were then washed with acetone, isopropanol, and distilled water for 5 min by using ultrasonic bath. To ensure removal of any debris that might have been introduced during cutting, these samples were rinsed twice with distilled water and then washed with 70% industrial methylated spirit (IMS) for 5 to 10 min, before being placed in a class II cell culture hood for ultraviolet sterilisation. These were kept in the UV hood for 30 min each side. After sterilisation, samples were placed in 48 well plate and washed 3 times for 5 min per wash with sterile phosphate buffer saline solution (PBS) to remove any possible residues of IMS.

MG63 cells (passage 6) were washed using PBS, and then 1 ml of enzyme solution (which is made of 100 ml sterile phosphate buffered saline, 1.5 ml of Trypsin (0.2% Trypsin with ethylene diamine tetra-acetic acid (EDTA)) was used to detach the cells from the surface. A seeding density of 40,000 cell/cm^2 was added to each sample. 250 μl of cell suspension was added to each well, also 300 μl of warmed (37 °C) media was added. These well plates were then incubated at 37 °C and 5% CO_2.Three samples (n = 3) of each coating were cultured for 3 and 7 days. After 2 days of seeding (and then again after 2 days) the media was changed which was consisted 500 ml of DMEM (Dulbecco's Modified Eagle Medium); foetal bovine serum (50 ml); L-glutamine (5 ml); antibiotics-antimycotics AA/AM (10 ml); HEPES buffer (10 ml); non-

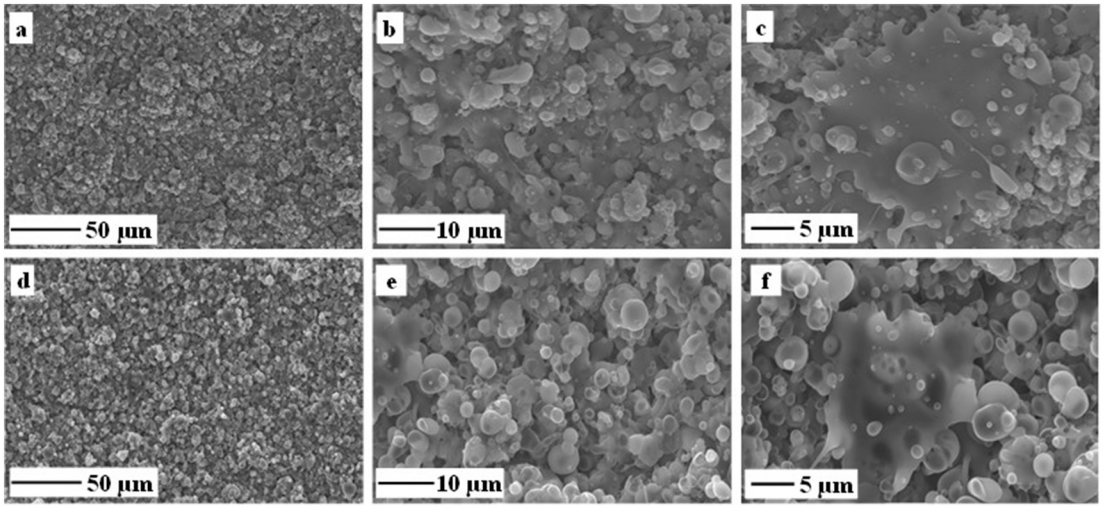

Fig. 2. Secondary electron microscope images showing the surface morphology of the coatings deposited at 50 kW: (a) & (b) ICIE-16 and (c) & (d) 13-93 coatings.

essential amino acids (5 ml) and ascorbic acid (75 mg). Cell viability was assessed using alamar blue assay (alamar blue concentrate: Hanks' Balanced Salt solution is 1:10), while, in order to evaluate the cell morphology, the samples were prepared by following fixation and dehydration based on different ethanol concentration. 3% glutaraldehyde in 0.1 M sodium cacodylate buffer was used as fixative. After 30 min, 0.3 ml of sucrose was added to the samples and refrigerated at 4 °C overnight. After this, the samples were washed three times (5 min each wash) with 0.1 M cacodylate buffer. Osmium tetroxide (1% solution) was added to the samples for 45 min. After this osmium tetroxide was removed and the samples were dehydrated with different concentration of ethanol (20%, 40%, 60%, 70%, 80%, 90% and 100%) then dried via hexamethyledisilazane overnight. Then, after gold coating, the samples were observed with SEM (JEOL 6490, Tokyo, Japan) at 20 kV with 10 mm working distance in SE imaging mode).

Statistical analysis was performed by prism graph pad (2365 Northside Dr. Suite 560 San Diego, USA). The p-value was calculated by single factor ANOVA Tukey post-test to determine the significance of the results with a significance level of <0.05.

3. Results

3.1. Powder characterisation

The ICIE16 bioactive glass powder had a particle size distribution of D_{10} = 1 μm, D_{50} = 4.5 μm and D_{90} = 11.4 μm (Fig. 1a), while 13-93 powder had a distribution of D_{10} = 0.8 μm, D_{50} = 2.7 μm and D_{90} = 11 μm (Fig. 1c).

SEM imaging of ICIE16 powder after ball milling (Fig. 1b) showed angular shaped particles, some larger than 10 μm. SEM analysis of the 13-93 bioactive glass (Fig. 1d) showed that most of the particles were finer, however particles larger than 10 μm were observed too.

3.2. Characterisation and morphology of the coatings

Fig. 2 shows the coating surface morphology of ICIE16 and 13-93 bioactive glasses sprayed at 50 kW. The surface of the ICIE16 coating is given in Fig. 2a and no globules can be seen on the surface of this coating. The high magnification image (Fig. 2b) of the surface shows that this coating surface consisted of molten splats with small round unmelted particles embedded in it; well-flattened splats of size larger than 20 μm (Fig. 2c) were also detected. The 13-93 bioactive glass

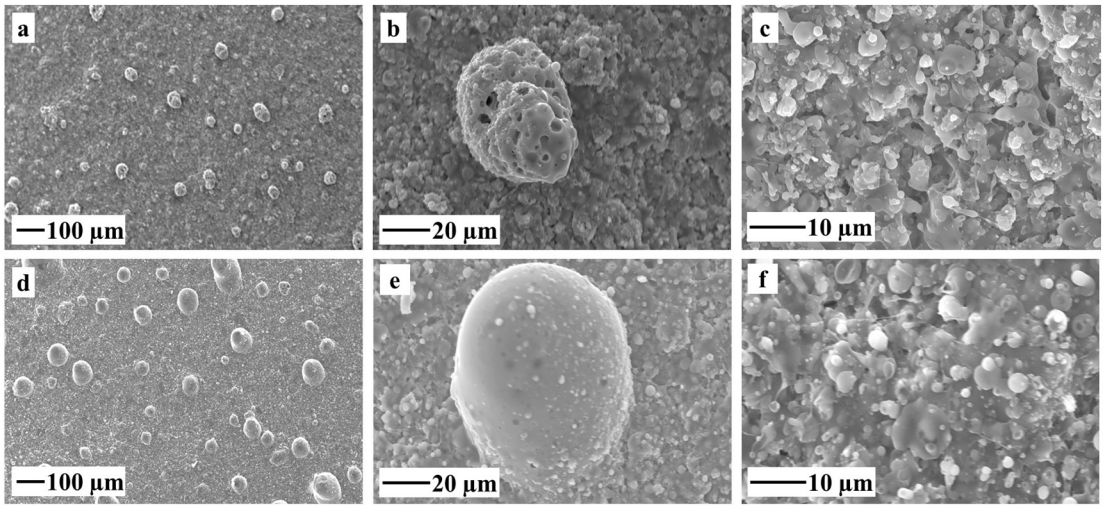

Fig. 3. Secondary electron microscope images showing the surface morphology of the coatings deposited at 75 kW flame power: (a), (b) and (c) represent ICIE- 16 and (d), (e), (f) represent 13-93 coatings.

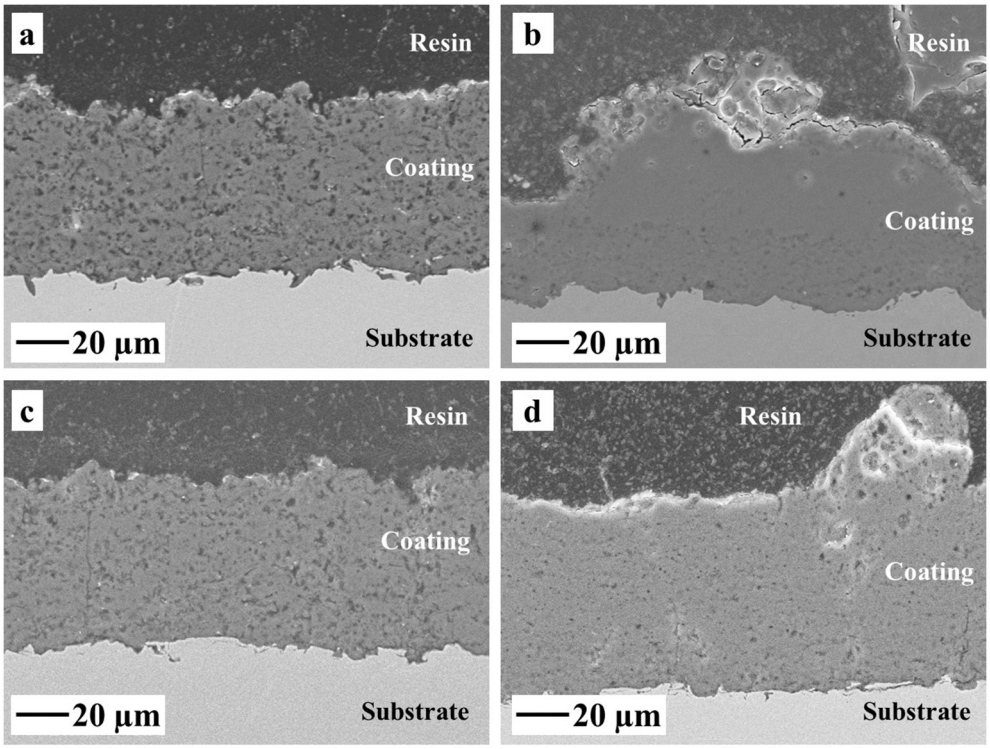

Fig. 4. Cross-sectional SEM images of the coatings deposited: ICIE16 coatings (a) deposited at 50 kW, (b) deposited at 75 kW, 13-93 coatings (c) deposited at 50 kW, and (d) at 75 kW.

Table 3
Physical and mechanical properties of ICIE16 and 13-93 coatings (mean value ± standard error).

Flame power (kW)	Thickness (µm)		Porosity (%)		Microhardness (HV)		Surface roughness (µm)	
	ICIE16	13-93	ICIE16	13-93	ICIE16	13-93	ICIE16	13-93
50	68 ± 1	67 ± 1	5 ± 1	6 ± 0.3	250 ± 8	246 ± 4	1.8 ± 0.1	2.4 ± 0.4
75	59 ± 10	62 ± 14	4 ± 0.5	3.5 ± 0.2	301 ± 10	318 ± 12	3.7 ± 0.3	6.5 ± 0.6

coating surface can be seen in Fig. 2d, which shows the absence of globules, while the high magnification image of this coating (Fig. 2e) shows that the surface presented a higher amount of round unmelted particles and also flattened splats, which were around 10 µm in diameter (Fig. 2f). The ICIE16 coating presented a surface roughness of $R_a = 1.8 \pm 0.1$ µm, while the surface roughness of 13-93 coating was slightly higher, $R_a = 2.4 \pm 0.4$ µm rough. This could be related to a greater presence of the partially molten particles on the surface of 13-93 coating (Fig. 2c).

The surface of the ICIE16 coating sprayed at 75 kW showed the presence of large humps over the surface (see Fig. 3a). A closer view (see Fig. 3b) revealed that those humps were spherical deposits with a porous structure and a diameter around 20 µm. Beyond the humps, the surface revealed a combination of flattened lamellae and fine partially melted particles (see Fig. 3c). The surface of the 13-93 coatings deposited at 75 kW revealed similar features; presenting large humps on the entire surface of the coating (see Fig. 3d). These semi-spherical shapes were not as porous as those observed on the surface of the ICIE16 coatings deposited at the same power (i.e. 75 kW), and were also larger in size with a diameter around 40 µm, with fine particles adhered to the surface (see Fig. 3e). The 13-93 coatings also contained well flattened lamellae with some rounded particles (see Fig. 3f). The surface of these two coatings was rougher than the coatings deposited at 50 kW, as the 75 kW coating of ICIE16 had roughness of 3.7 ± 0.3 µm. Similarly, the surface of 13-93 coating deposited at 75 kW coating had a surface roughness of 6.5 ± 0.6 µm.

Table 4
EDX analysis on the top of as sprayed surfaces of ICIE16 and 13-93 coatings (where R50 is the coating deposited at 50 kW and R75 at 75 kW flame power. In addition, the elemental wt% of the starting powder also from EDX analysis is included).

Element (wt%)		Na	Si	P	K	Ca	Mg
ICIE16	Nominal composition	4.8	22.3	1.1	8.3	23	–
	Powder	5.0 ± 0.1	25.0 ± 0.6	1.1 ± 0.1	8.9 ± 0.2	18.0 ± 2.0	–
	R50	3.0 ± 0.4	26.0 ± 0.3	1.0 ± 0.1	4.0 ± 0.1	24.0 ± 0.2	–
	R75	2.0 ± 0.2	28.0 ± 0.1	0.7 ± 0.01	3.0 ± 0.1	26.0 ± 0.3	–
13-93	Nominal composition	4.3	24.3	1.8	9.8	14	2.9
	Powder	5.0 ± 0.1	25.0 ± 0.05	1.6 ± 0.1	10.0 ± 1	14.0 ± 0.3	3.0 ± 0.3
	R50	2.3 ± 0.3	28.0 ± 0.4	1.0 ± 0.1	6.0 ± 0.6	16.0 ± 1.0	3.0 ± 0.1
	R75	1.0 ± 0.5	29.4 ± 0.1	1.0 ± 0.0	4.0 ± 0.1	19.0 ± 0.7	3.6 ± 0.1

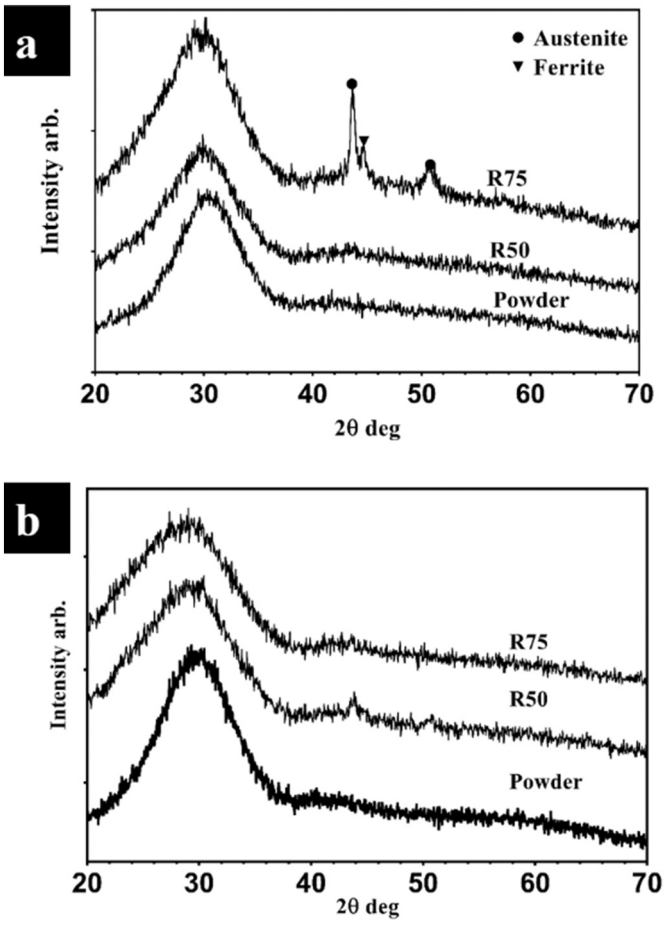

Fig. 5. XRD scans (a) of ICIE16 and (b) 13-93 bioactive glass powders and coatings deposited at 50 kW and 75 kW.

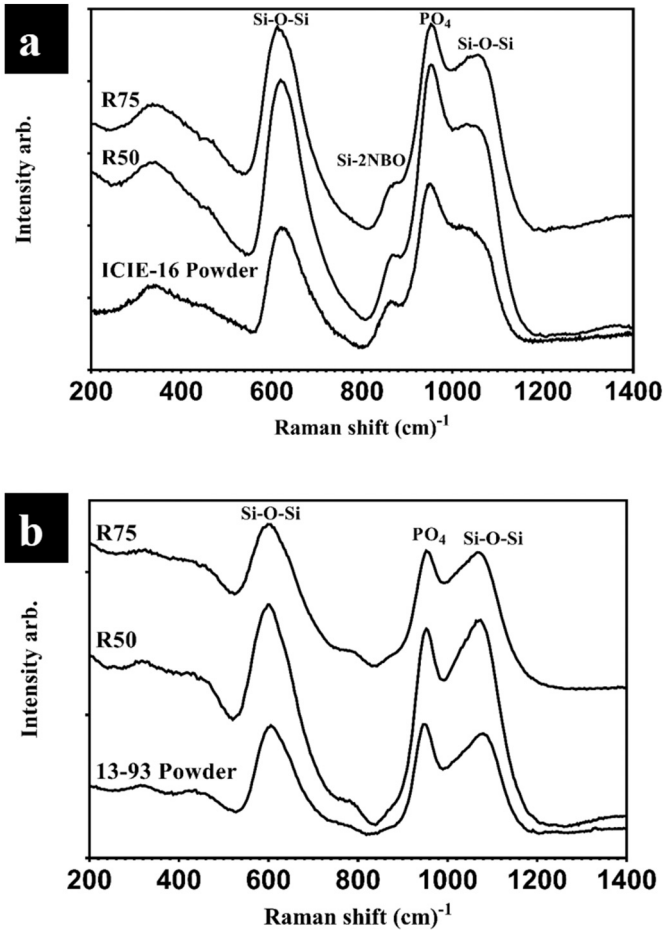

Fig. 6. Raman analysis (a) of ICIE16 and (b) 13-93 bioactive glass powders and coatings deposited at 50 kW and 75 kW.

All the coatings produced did not reveal any delamination at the coating-substrate interface as can be seen from the cross-sectional images (see Fig. 4). In addition, they presented a uniform coating thickness where some remnant porosity was detected. Also, some globular features in the ICIE16 and 13-93 coatings deposited at 75 kW were noticed (Fig. 4b and d).

The physical and mechanical properties of the ICIE16 and 13-93 coatings are shown in Table 3. Vickers microhardness testing revealed very similar values for both bioactive glass coatings deposited at 50 kW flame power (i.e. 250 ± 8 HV for ICIE16 and 246 ± 4 HV for 13-93). However, both of the glass coatings deposited at 75 kW revealed higher microhardness values (i.e. 301 ± 10 HV for ICIE16 and 318 ± 12 HV for the 13-93 coating).

EDX surface analysis of ICIE16 coatings can be seen in Table 4, which shows that increasing flame power had an effect on the glass composition. The Si content (wt%) was observed to vary slightly from 25 wt% for the initial powder to 26 wt% in the 50 kW samples and up to 28% for the 75 kW samples. The Na content was observed to vary from 5 wt% in the initial powder to 3 and 2 wt% when sprayed at 50 and 75 kW flame power, respectively. A similar trend was observed in the of Ca content that increased from 18 wt% to 24 and 26 wt% with the increase of flame powers from 50 to 75 kW. Wt% of P remained approximately constant and presented a similar wt% in the starting powder and in the samples sprayed at both flame powers. K however revealed a higher variability in comparison to the starting powder from between (8.9 wt%) to 4 wt% and 3 wt% when deposited at 50 and 75 kW.

EDX area analysis of the top surface of the 13-93 coatings is provided in Table 4, which shows that after spraying the Na content had reduced from 5 wt% to 2 wt% and 1 wt% after spraying at 50 and 75 kW. Mg and P remained constant at 3 wt% and 1 wt% after spraying at both the different flame powers employed; however, K showed the same trend as Na, with reductions observed with increasing flame power from 6 wt% at 50 kW to 4 wt% at 75 kW flame power.

The ICIE16 and 13-93 bioactive glass powders and the as sprayed coatings were studied by XRD analysis to explore any possible phase transformation occurring during spraying (Fig. 5). No crystallization peaks were detected in any of the diffractograms (with the exception of signal from the stainless steel substrate in the case of ICIE16), and only a broad hump typical of amorphous glass structures was observed between 25° and 35° [30] [31] confirming that the amorphous nature of the starting materials had been preserved in the as sprayed coatings.

Raman analysis of both glass composition coatings revealed close similarities to that of the original powders (see Fig. 6). For all coatings and powders, the bands at 621 cm^{-1} and 1057 cm^{-1} were assigned to the stretching of Si-O-Si [32]. Whereas, bands at 950 cm^{-1} were associated with the stretching of PO_4^{-2} [32,33]. However, the spectra of ICIE16 coatings and powder revealed a peak at 886 cm^{-1} (see Fig. 6a), which was associated to the non-bridging oxygen silica [32]; this band was not present in the Raman analysis of 13-93 powder and coatings. There was also a shoulder in the Raman spectra of 13-93 coatings and powder at 786 cm^{-1} which was related to MgO [34].

3.3. Simulated body fluid tests

The SBF tests and subsequent SEM analysis of the ICIE16 coatings revealed the formation on the surface of "cauliflower" like structure which are characteristic of HA deposits post immersion in SBF. This

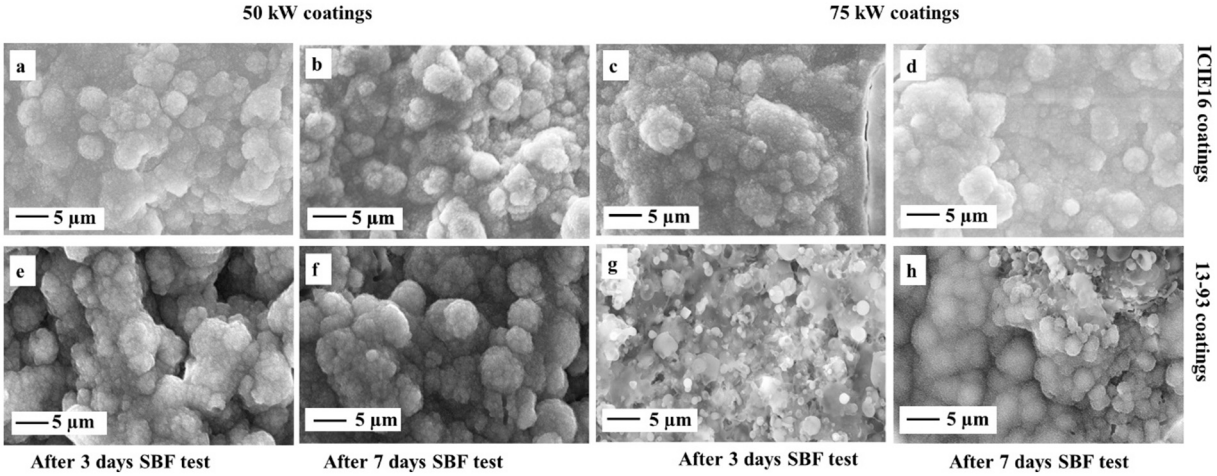

Fig. 7. Secondary electron microscope images showing the surface morphology of the coatings after 3 days immersing in SBF solution (a), (c) and (e), (g) and after 7 days immersing (b), (d) and (f), (h); while (a), (b) and (e), (f) at 50 kW and (c), (d) and (g), (h) at 75 kW flame power. a, b, c and d are ICIE16 coatings while e, f, g, h are 13-93 glass coatings.

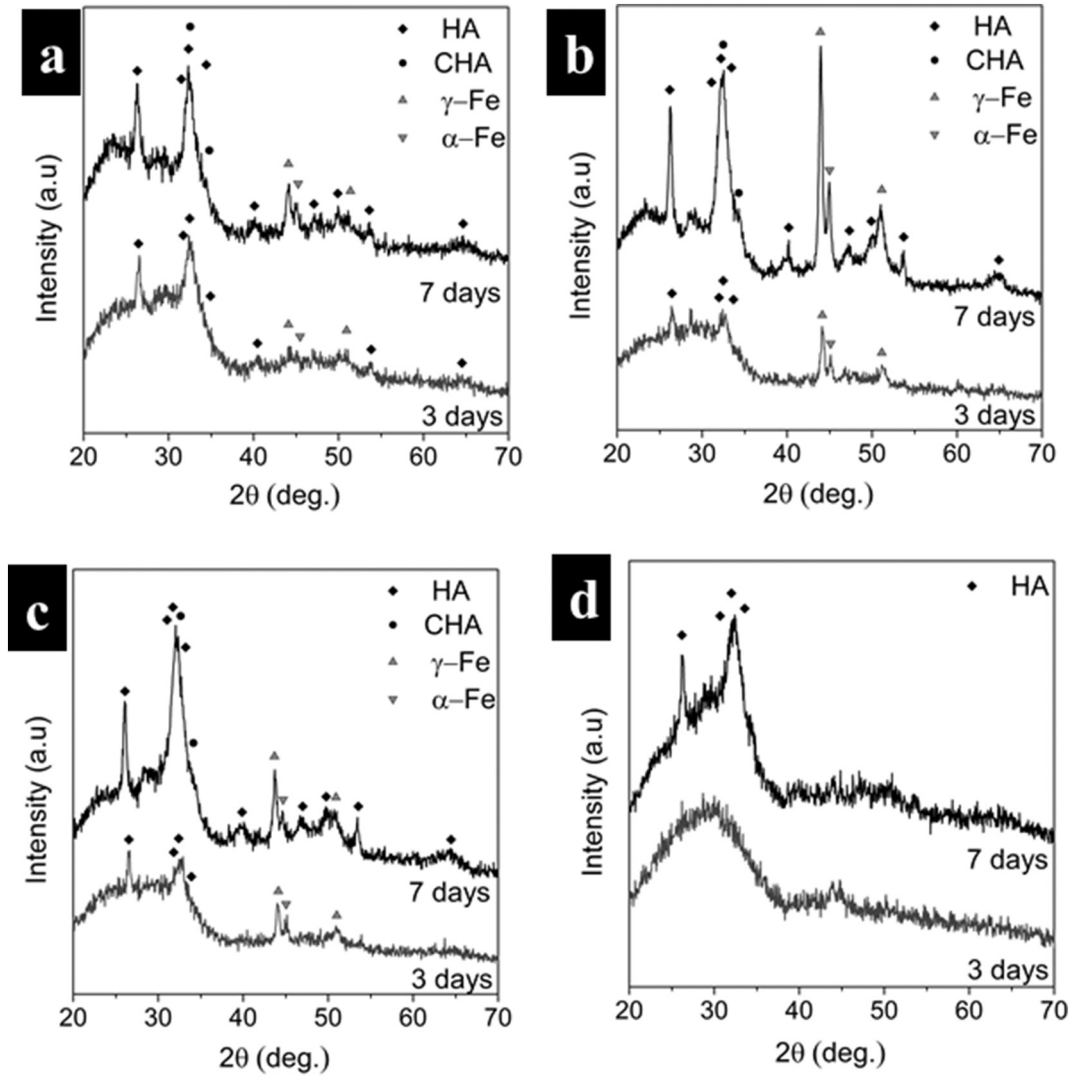

Fig. 8. XRD scan after 3 and 7 days of soaking in SBF solution, (a) and (b) ICIE16 coatings sprayed at 50 and 75 kW respectively; (c) and (d) 13-93 coatings sprayed at 50 and 75 kW, respectively. (SEE Fig. 6 for the as- sprayed XRD.)

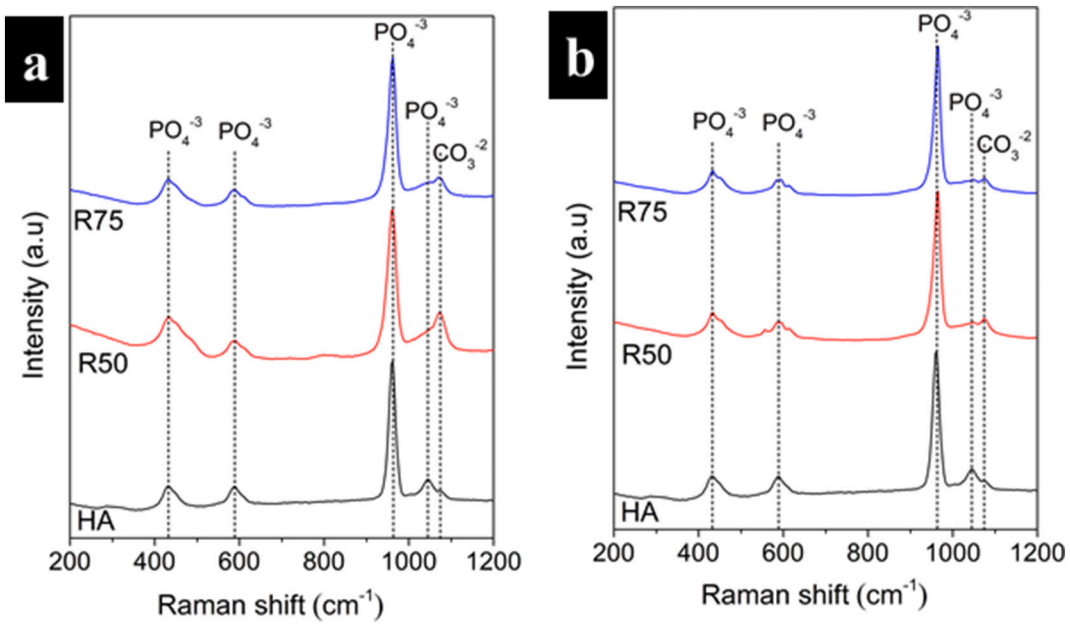

Fig. 9. Raman spectra acquired on the surfaces of the S-HVOF thermal spray deposited bioactive glass coatings at flame powers of 50 kW and 75 kW after 7 days of immersion in SBF (a) ICIE16 coatings, (b) 13-93 coatings.

structures had formed on ICIE16 coatings obtained using different flame power (50 and 75 kW) just after three days of immersion in SBF (see Fig. 7a and c), and could be more easily identified after 7 days of immersion in SBF (Fig. 7b and d). The surface morphology of the 13-93 coating samples deposited at 50 kW followed a similar pattern (see Fig. 7e for deposition after 3 days and Fig. 7f for deposition after 7 days of immersion in SBF). Instead, the 13-93 coatings deposited at 75 kW did not reveal any HA deposition on its surface after 3 days of immersion in SBF (see Fig. 7g). However, after immersion in SBF for 7 days, some "cauliflower" like structure was detected on the surface of this coating; however, the surface was not fully covered with HA (see Fig. 7h).

The XRD patterns shown in Fig. 8 revealed that, after 3 days of immersion in SBF, all the samples had formed HA (PDF #72-1243), except the 13-93 coating deposited at 75 kW, which developed HA after 7 days. The broad peaks of 26° and 32° identify HA presence; the broadening of these peaks is associated with the nanocrystalline structure of the precipitated HA. In addition, the overlapping with the main peaks of carbonated hydroxyapatite (HCA) (PDF #19-10272), detected also from the Raman spectrum (Fig. 9), also contributed to this broadening effect [25]. The intensity of these peaks increased with longer immersion times up to 7 days. Peaks belonging to the stainless steel substrate (austenite PDF #33-0397 and ferrite PDF #87-0721) can also be detected in some diffractograms.

Consistent with these results, the Raman spectra measured from the top surface of all coatings immersed in SBF for 7 days resembled the spectrum of synthetic HA powder (Fig. 9). The peak at 960 cm^{-1} in the spectra was assigned to symmetric stretching v_1 of PO_4^{-3}. The broad peak at 432 cm^{-1} was assigned to v_1 bending of PO_4^{-3}. Whereas the broad peak at 585 cm^{-1} was due to the anti-symmetric bending v_4 of PO_4^{-3} [35]. The peaks at 1045 cm^{-1} for the HA powder were assigned to vibration of the PO_4^{-3} v_3. The peak at 1070 cm^{-1} was assigned to the stretching v_1 mode of carbonate CO_3^{-2} groups which was probably due to the precipitated HA, as it was not present in the spectrum of synthetic HA. This also confirmed the carbonated nature of the precipitated HA of the coating surfaces [36]. Fig. 9b shows the Raman spectra of 13-93 coatings deposited at 50 and 75 kW flame power immersed in SBF for 7 days, the analysis showed that there was a small peak in the spectrum of 50 kW coating at 556 cm^{-1}. Also, Raman spectra of both 13-93 coatings after immersed in SBF for 7 days showed that there was a band at 584–596 cm^{-1} and a shoulder at 614 cm^{-1}. These peaks and shoulders were due to the v_4 bending of PO_4^{-3} [37].

To show the compositional changes of the produced coating after 7 days of immersion in SBF, EDX scans in the coating cross section are reported in Fig. 10; the EDX scans were taken at different points along a perpendicular line from the coating substrate interface to the top surface of the coating. Fig. 10a shows the cross section of ICIE16 coating deposited at 50 kW, while Fig. 10b representing the corresponding EDX analysis. The coating thickness was initially 68 ± 1 μm before immersion in SBF, and after immersion for 7 days the thickness had reduced to approximately 57 ± 1.5 μm while the deposited HA layer on this residual coating was approximately 9 ± 1 μm (see Fig. 10a). The ICIE16 coating deposited at 75 kW was 59 ± 10 μm, and also reduced to 45 ± 13 μm, while the precipitated HA layer (after 7 days of immersion in SBF) on the surface of this coating was approximately 13 ± 3.5 μm (see Fig. 10c). EDX analysis of this coating (Fig. 10d) showed that Ca was observed to be 32 wt% and P was 18 wt% in the deposited HA layer.

The 13-93 coating deposited at 50 kW was initially 67 ± 1 μm, and after soaking in SBF for 7 days reduced to 58 ± 2 μm (Fig. 10e) while the precipitated HA layer was 8.5 ± 4.3 μm thick. Fig. 10f shows that Ca content was 32 wt% and P was 17 wt% in the precipitated HA layer. The 75 kW 13-93 bioactive glass coating was 62 ± 14 μm prior to immersion in SBF, but was not uniformly distributed across the surface even after 7 days as noted above. The thickness of this residual coating was 60 ± 5 μm, and the precipitated HA thickness was approximately 6 ± 1 μm (see Fig. 10g). Fig. 10h showed that Si content remained constant at 30 wt% throughout the coating, and then started decreasing at the coating- HA interface to almost 15 wt% at the top of the HA layer. Similarly, the Ca content did not change in the coating and remained at around 15 wt%, which then started increasing at the coating- HA layer to almost 25 wt% in the deposited HA layer. The P content showed the same trend as Ca and remained constant at 2 wt% in the coating, starting to increase at the interface between coating and HA layer to almost 15 wt% at the top of HA layer.

Ca/P atomic ratio of the ICIE16 coatings before SBF and after immersion in SBF for 3 and 7 days can be seen in Table 5. It was observed that the Ca/P ratio decreased after the SBF tests. Before SBF tests it was 27.0 ± 2.0 for 50 kW coating and 28.5 ± 1.6 for 75 kW coating. After immersion in SBF for 3 days this had decreased to 1.78 ± 0.03 and 2.23

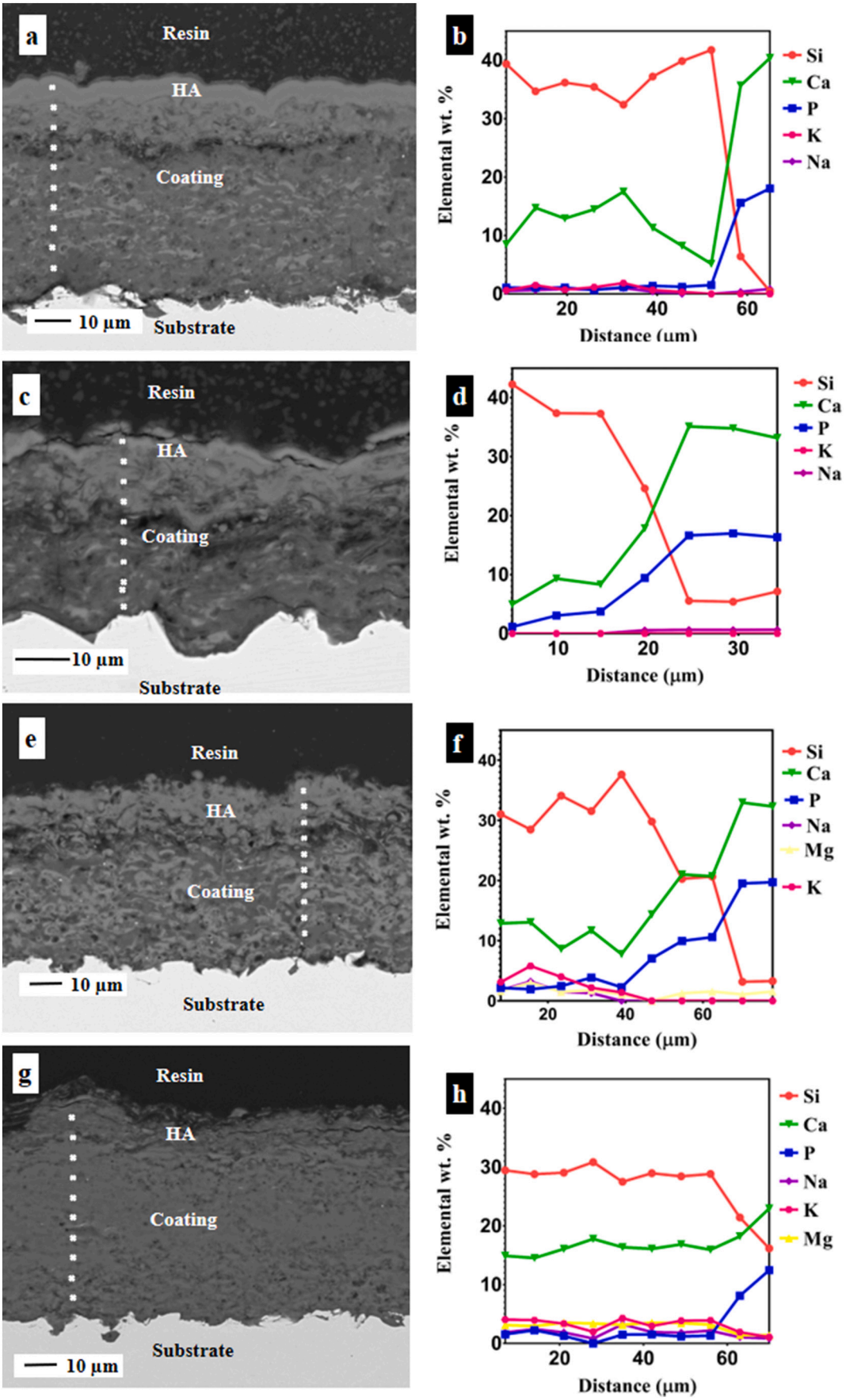

Fig. 10. a, c, e, g are BSE images while b, d, f and h are the respective EDX line scan of ICIE16 and 13-93 coatings deposited at 50 and 75 kW after immersion in SBF 7 days.

Table 5
Ca/P ratio (atomic %) of the ICIE16 and 13-93 as sprayed coatings and soaking in SBF after 3 and 7 days.

Flame power	Ca/P ratio for ICIE16 coatings			Ca/P ratio for 13-93 coatings		
	0 days	3 days	7 days	0 days	3 days	7 days
50	27.0 ± 2.0	1.78 ± 0	1.71 ± 0	11.9 ± 2.5	1.55 ± 0.04	1.24 ± 0.06
75	28.5 ± 1.6	2.23 ± 0	1.55 ± 0	11 ± 0.6	12.7 ± 1.25	2.05 0.74

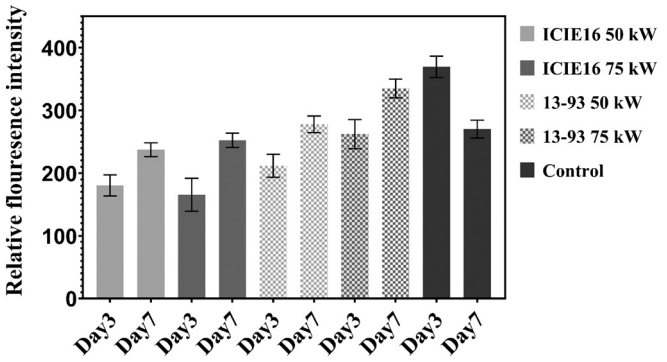

Fig. 11. In vitro viability alamar blue assays on MG 63 cells, after 3 days and 7 days of incubation.

± 0.08 for 50 and 75 kW coatings. These values further decreased to 1.70 ± 0.05 for the 50 kW coating and 1.55 ± 0.01 for the 75 kW coating after immersion in SBF for 7 days.

The Ca/P atomic ratio for the 13-93 coatings before and after SBF tests is given in Table 5. This ratio was 11.9 ± 2.5 for 50 kW coating and 28.5 ± 1.6 for the 75 kW coating. After immersion in SBF for 3 days the Ca/P ratio for 50 kW coating decreased to 1.55 ± 0.04. However the 75 kW coating remained at approximately 12.7 ± 1.2. Further immersion in SBF for 7 days revealed that this ratio decreased to 1.24 ± 0.06 for the 50 kW coating and to 2.05 ± 0.74 for the 75 kW coating.

3.4. In vitro cell interaction

Cell viability and proliferation tests were performed on ICIE16 and 13-93 bioactive glass coatings at two different time points of 3 and 7 days. Results from alamar blue assay are summarised in Fig. 11. Two repeats of experiments were performed, and both of these were comparable in terms of cell viability, moreover significant differences were ($p < 0.05$) present between control and any of the coating at time point of 3 days and the intensity was higher for the control than the coatings. However, no significant differences ($p > 0.05$) were present between control and any of the coating when 7 days were elapsed. After 7 days, it can be seen that the intensity was higher for all the coatings compared to after 3 days, which indicates that cells proliferated on coating surfaces. From Fig. 11 it should be noted that 13-93 coating which was deposited at 75 kW showed highest intensity (more than the control) at time point 7, which means that cell response was better towards this coating in comparison to the other three coatings.

Fig. 12 shows the morphology of MG63 cells adhered on to ICIE-16 and 13-93 bioactive glass coatings. After 3 days of incubation, it can be seen from Fig. 12a, b, e and f that cells were growing on the surfaces of the coatings and demonstrated extended lamellipodia and filopodia, however, as can be seen from Fig. 12b and f (which are SEM images of the ICIE16 and 13-93 coatings deposited at 75 kW of flame power after 3 days of incubation), multilayer cells were present on these surfaces. By increasing incubation time (Fig. 12c, d, g and f) the surfaces of all coatings appeared to be covered with sheets of cells. Also, the cracks in sheets were due to dehydration of the samples for SEM observation.

4. Discussion

4.1. Microstructure of ICIE16 and 13-93 bioactive glass coatings

Regardless of the glass formulations tested or the flame power applied, all the coatings adhered to the substrates, as no cracks were present along the coating-substrate interface. It should be noted that this was the first ever attempt reported in the literature to develop coatings from these compositions. ICIE16 and 13-93 bioactive glasses coatings obtained after spraying at a flame power of 50 kW had similar microstructure; however, comparing the surface roughness, the 50 kW ICIE16 coating surfaces were smoother than the 13-93 bioactive glass coating deposited at the same flame power. This could be due to the different particle size distribution of the two glasses used for spraying. As 13-93 bioactive glass powder contains a higher fraction of fine particles (Fig. 1c) than in the ICIE-16 glass powder (Fig. 1a). It has been reported that fine particles, due to their low inertia, do not deform when hitting the substrate, instead they retain their spherical morphology due to surface tension [39]. The presence of more globular particles on the surface of the 13-93 glass 50 kW coating (Fig. 2c and d) also contributed to its roughness, in comparison to the ICIE16 bioactive glass coatings

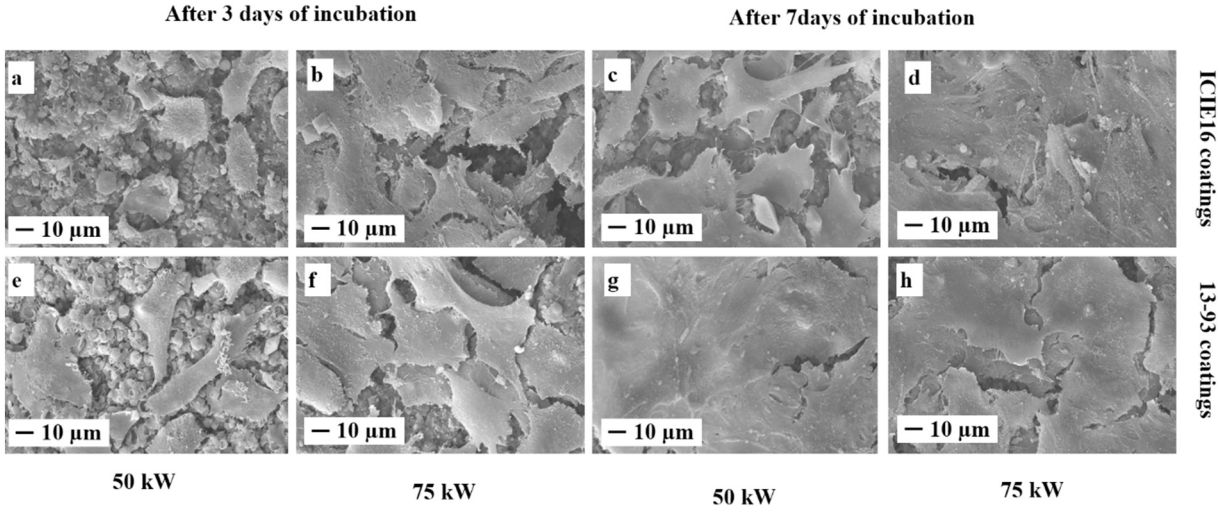

Fig. 12. SEM images of MG63 cells grown on ICIE16 (a-d) and 13-93 (e-h) bioactive glass coatings, a, b, e and f after 3 days of seeding and c, d, g and h after 7 days of seeding. a, c, e, and g are the coatings deposited at 50 kW and b, d, f and h are deposited at 75 kW of flame power.

deposited at the same power (Fig. 2a and b).

The surfaces of the ICIE16 and 13-93 bioactive glass coatings deposited at high flame power (75 kW) had semi-spherical features (Fig. 3). This could have been caused by large agglomerates forming inside the combustion chamber during spray and adhering to the chamber walls. At high flame power, these agglomerates can melt, due to higher heat transfer, leading to detachment from the walls of the combustion chamber, and can be sprayed onto the substrate [38]. These globules were also mainly responsible for the high surface roughness of the higher flame power coatings [39] as compared to the lower 50 kW coatings [40]. However, the globules present on the surface of 13-93 coating were not as porous (Fig. 3e) as those present on the surface of ICIE16 coating deposited at 75 kW (Fig. 3b), where it seems that a skin formed over the pores. This could be attributed to the potential differences in viscosity of 13-93 and ICIE16 glasses. However, a study by Döhler et al. investigated that these glasses were very similar in viscosity profiles [8].

The cross-sectional view of ICIE16 75 kW coatings (Fig. 4b) showed that globules were cone shaped and porous. After the porous structure at the base of the cones, a dense region was present in the middle of these globules. By studying the morphology of these globular shapes, it can be argued that they started as small surface disruptions. Subsequently, the incoming melted particles interact with these deviations, resulting in larger porous regions due to localised splat disorder. With each torch pass, splat/perturbation interaction repeats creating more porosity. The middle of these globules was dense, probably due to the decrease of the radius of the curvature [39]. For both glass compositions ICIE16 and 13-93, the coatings obtained at a flame power of 75 kW were thinner and with a lower porosity than the coatings obtained at 50 kW (Fig. 4). This was due to the higher melting degree of the glass particles at higher flame power, which leads to coatings that are less porous and with higher microhardness values than the coatings obtained at a lower flame power [41,42].

4.2. Apatite layer formation of ICIE16 and 13-93 coatings in SBF

Investigation of the coatings after immersion in SBF revealed the development of cauliflower-like precipitates on their surfaces which are characteristic of HA deposition and growth in SBF [43,44]. The broad crystalline peak between 26° and 32° were associated with the nano-crystalline nature of the precipitated HA [45]. HA formed just after 3 days of immersion in SBF on the surfaces of both glass composition coating deposited at 50 kW as confirmed via XRD (Fig. 8a and c). However, no HA was observed on the surface of 13-93 coating deposited at 75 kW after 3 days of immersion in SBF (Fig. 8d). This coating revealed HA deposition only after 7 days of immersion in SBF (Fig. 8d). Due to a higher SiO_2 content, 13-93 glass is comparatively resistant to dissolution and hence apatite formation [9]. In addition, the presence of MgO also makes this glass less vulnerable to dissolution [46]. The 13-93 coating deposited at 75 kW has more SiO_2 and MgO relative to the starting powder (Table 4), which could also have contributed to delayed apatite formation [46]. MgO in glass formulations has been reported to decrease HA formation in vitro [16]. However, in-vivo it has been shown to support early stage mineralisation [16,58]. MgO acts as network intermediate [16] thus inhibiting the dissolution process, which showed to be low for 13-93 compared to Bioglass® and ICIE16, due to the higher silica content [11].

Both ICIE16 coatings showed more pronounced compositional changes in SBF than 13-93 coatings as suggested by EDX analysis along the cross section of the coatings after immersion in SBF for 7 days (Fig. 10). This difference in reactivity of the ICIE16 and 13-93 coatings deposited at 50 kW was probably due to the higher content of silica in 13-93 than ICIE16 (Table 1), which makes 13-93 more stable in SBF as previously discussed [9]. Also ICIE16 composition is closer to Bioglass® (which is the most bioactive material known) as can be seen in the ternary phase diagram described by Hench et al. [47], and this could explain the more pronounced compositional changes of ICIE16 coating in comparison to 13-93 coating. However, comparing the 50 kW coating and 75 kW of ICIE16 it was observed that the 75 kW coating showed more reactivity than the coating produced at 50 kW, which may be due to the higher surface roughness presented by the 75 kW coating. It has been shown that higher surface roughness increases the contact area with SBF [48], which increases ion leaching from bioactive coatings [22]. On the other hand, the 75 kW coating of 13-93 showed less reactivity than the 50 kW coating during the SBF test. The reason for the lower reactivity of 13-93 coating deposited at 75 kW is the same as for the coating deposited at 50 kW, i.e. high silica content and low bioactivity, in comparison to ICIE16 coating which is the composition closer to Bioglass®.

4.3. In vitro cell interaction of ICIE-16 and 13-93 bioactive coatings

In this work, through the study of MG63 cells, it was shown that ICIE16 and 13-93 coatings deposited via SHVOF thermal spray on stainless steel substrate were cytocompatible, as the coatings showed no cytotoxicity and displayed good proliferation. From proliferation results it can be stated that both coatings supported an increased viability across the length of the study. However, it should be noted that the 13-93 coating deposited at 75 kW showed highest intensity after 7 days of incubation compared to the other coatings (Fig. 11). This could be attributed to the rougher surface of this coating (6.5 ± 0.6 μm) and the literature shows that rough surfaces can significantly enhance the attachment of osteoblast-like MG 63 cells [49]; however, this effect was noted only during the first 24 h of incubation and did not affect their proliferation rate. The same effect of surface roughness on cells was also reported by Bovan et al. [50]. Also from the proliferation results, intensity for the 75 kW coating of 13-93 bioactive glass was more than that of the control, which may be due to the enhanced cell proliferation owing to the presence of MgO in the glass composition as Mg can directly enhance osteoblast proliferation [51]. From these results, it can be concluded that both ICIE16 and 13-93 coatings deposited at 50 and 75 kW were nontoxic and bioactive.

5. Conclusions

Bioactive coatings of ICIE16 and 13-93 compositions with varied apatite forming ability were successfully produced by an emerging SHVOF thermal spraying technique. Change of flame powers for the same glass resulted in different microstructure of the coatings, and hence differences in the reactivity in SBF. Spraying at same flame power but with different compositions also resulted in different microstructure and apatite forming ability when tested using SBF. In-vitro cell culture tests showed that the surfaces of these coatings were biocompatible with human osteoblast-like (MG-63) cells.

It can be concluded that the ICIE16 coatings were more reactive in SBF than the 13-93 coatings, although both were deemed to be biocompatible. Since the formation of HA in SBF on the surface of bone related biomaterials is considered to be evidence of its bioactivity, based on the results above, it can be concluded that the ICIE16 coatings would be better coating materials to achieve enhanced bonding between the host tissue and orthopaedic related implants, in comparison to the 13-93 coatings. However, with 13-93 comparatively stable coatings, it is possible to obtain coatings that could survive for longer time in physiological environment.

Declaration of competing interest

The authors declare that they have no known competing financial interests or personal relationships that could have appeared to influence the work reported in this paper.

Acknowledgment

This work was supported by the Engineering and Physical Sciences Research Council [EP/N50970X/1]. Saira Bano acknowledges a fully funded Faculty of Engineering Research Excellence PhD scholarship for international students by University of Nottingham UK (sponsor licence number RFDX42DB2, scholarship ref. number: 16453). Saira Bano is a lecturer at the University of Engineering and Technology Peshawar, Pakistan. We acknowledge support from Mr. John Kirk for thermal spray experiments and Dr. Federico Venturi for editorial support. We gratefully acknowledge technical support from Julie Thompson and Louise Briggs in cell culture tests, as well as the Nanoscale and Microscale Research Centre at University of Nottingham for access to the SEM and Raman spectroscopy facilities.

References

[1] M. T. Islam, R. M. Felfel, E. A. Abou Neel, D. M. Grant, I. Ahmed, and K. M. Z. Hossain, "Bioactive calcium phosphate–based glasses and ceramics and their biomedical applications: A review," J. Tissue Eng., vol. 8, 2017, doi: https://doi.org/10.1177/2041731417719170.

[2] L.L. Hench, R.J. Splinter, W.C. Allen, T.K. Greenlee, Bonding mechanisms at the interface of ceramic prosthetic materials, J. Biomed. Mater. Res. 5 (6) (1971) 117–141, https://doi.org/10.1002/jbm.820050611.

[3] J.P. Borrajo, et al., The role of the thickness and the substrate on the in vitro bioactivity of silica-based glass coatings, Mater. Sci. Eng. C 25 (2) (2005) 187–193, https://doi.org/10.1016/j.msec.2005.01.015.

[4] L.L. Hench, The story of Bioglass®, J. Mater. Sci. Mater. Med. 17 (11) (2006) 967–978, https://doi.org/10.1007/s10856-006-0432-z.

[5] A. Nommeots-nomm, P.D. Lee, J.R. Jones, Direct ink writing of highly bioactive glasses direct ink writing of highly bioactive glasses, J. Eur. Ceram. Soc. 38 (3) (2018) 837–844, https://doi.org/10.1016/j.jeurceramsoc.2017.08.006.

[6] F. Baino, E. Verne, Glass-based coatings on biomedical implants: a state-of-the-art review, Biomed. Glas. 3 (1) (2017) 1–17, https://doi.org/10.1515/bglass-2017-0001.

[7] S. Bano, I. Ahmed, D. M. Grant, A. Nommeots-Nomm, and T. Hussain, "Effect of processing on microstructure, mechanical properties and dissolution behaviour in SBF of Bioglass (45S5) coatings deposited by Suspension High Velocity Oxy Fuel (SHVOF) thermal spray," Surf. Coatings Technol., vol. 372, no. May, pp. 229–238, 2019, doi: https://doi.org/10.1016/j.surfcoat.2019.05.038.

[8] F. Döhler, D. Groh, S. Chiba, J. Bierlich, J. Kobelke, D.S. Brauer, Bioactive glasses with improved processing. Part 2. Viscosity and fibre drawing, J. Non-Cryst. Solids 432 (2016) 130–136, https://doi.org/10.1016/j.jnoncrysol.2015.03.009.

[9] A. Nommeots-Nomm, et al., Highly degradable porous melt-derived bioactive glass foam scaffolds for bone regeneration, Acta Biomater. 57 (2017) 449–461, https://doi.org/10.1016/j.actbio.2017.04.030.

[10] I. Elgayar, A.E. Aliev, A.R. Boccaccini, R.G. Hill, Structural analysis of bioactive glasses, J. Non-Cryst. Solids 351 (2) (2005) 173–183, https://doi.org/10.1016/j.jnoncrysol.2004.07.067.

[11] M.N. Rahaman, et al., Bioactive glass in tissue engineering, Acta Biomater. 7 (6) (2011) 2355–2373, https://doi.org/10.1016/j.actbio.2011.03.016.

[12] M. Brink, T. Turunen, R.P. Happonen, A. Yli-Urpo, Compositional dependence of bioactivity of glasses in the system Na2O-K2O-MgO-CaO-B2O3-P2O5-SiO2, Journal of Biomedical Materials Research: An Official Journal of The Society for Biomaterials and The Japanese Society for Biomaterials 37 (1) (1997) 114–121, https://doi.org/10.1002/(SICI)1097-4636(199710)37:1<114::AID-JBM14>3.0.CO;2-G.

[13] D.S. Brauer, Bioactive glasses - structure and properties, Angew. Chemie - Int. Ed. 54 (14) (2015) 4160–4181, https://doi.org/10.1002/anie.201405310.

[14] A. Hoppe, et al., In vitro cell response to Co-containing 1393 bioactive glass, Mater. Sci. Eng. C 57 (2015) 157–163, https://doi.org/10.1016/j.msec.2015.07.014.

[15] E. Cañas, M. Vicent, M.J. Orts, R. Moreno, E. Sánchez, Bioactive glass suspensions preparation for suspension plasma spraying, J. Eur. Ceram. Soc. 36 (16) (2016) 4281–4290, https://doi.org/10.1016/j.jeurceramsoc.2016.06.011.

[16] G. Bolelli, V. Cannillo, R. Gadow, A. Killinger, L. Lusvarghi, J. Rauch, Investigation of High-Velocity Suspension Flame Sprayed (HVSFS) glass coatings, Ceram. - Silikaty 54 (1) (2010) 1–7, https://doi.org/10.1016/j.jeurceramsoc.2009.01.032.

[17] N. Stiegler, et al., High-velocity suspension flame sprayed (HVSFS) hydroxyapatite coatings for biomedical applications, J. Therm. Spray Technol. 21 (2) (2012) 275–287, https://doi.org/10.1007/s11666-011-9724-z.

[18] A. Killinger, M. Kuhn, R. Gadow, High-Velocity Suspension Flame Spraying (HVSFS), a new approach for spraying nanoparticles with hypersonic speed, Surf. Coatings Technol. 201 (5) (2006) 1922–1929, https://doi.org/10.1016/j.surfcoat.2006.04.034.

[19] A. Killinger, R. Gadow, G. Mauer, A. Guignard, R. Vaen, D. Stöver, Review of new developments in suspension and solution precursor thermal spray processes, J. Therm. Spray Technol. 20 (4) (2011) 677–695, https://doi.org/10.1007/s11666-011-9639-8.

[20] M. Bai, H. Maher, Z. Pala, T. Hussain, Microstructure and phase stability of suspension high velocity oxy-fuel sprayed yttria stabilised zirconia coatings from aqueous and ethanol based suspensions, J. Eur. Ceram. Soc. 38 (4) (2018) 1878–1887, https://doi.org/10.1016/j.jeurceramsoc.2017.10.026.

[21] J.W. Murray, A.S.M. Ang, Z. Pala, E.C. Shaw, T. Hussain, Suspension High Velocity Oxy-Fuel (SHVOF)-sprayed alumina coatings: microstructure, Nanoindentation and Wear, J. Therm. Spray Technol. 25 (8) (2016) 1700–1710, https://doi.org/10.1007/s11666-016-0462-0.

[22] G. Bolelli, et al., Comparison between suspension plasma sprayed and high velocity suspension flame sprayed bioactive coatings, Surf. Coatings Technol. 280 (2015) 232–249, https://doi.org/10.1016/j.surfcoat.2015.08.039.

[23] G. Bolelli, et al., Suspension thermal spraying of hydroxyapatite: microstructure and in vitro behaviour, Mater. Sci. Eng. C 34 (1) (2014) 287–303, https://doi.org/10.1016/j.msec.2013.09.017.

[24] G. Bolelli, et al., Deposition mechanisms in high velocity suspension spraying: case study for two bioactive materials, Surf. Coatings Technol. 210 (2012) 28–45, https://doi.org/10.1016/j.surfcoat.2012.08.046.

[25] L. Altomare, et al., Microstructure and in vitro behaviour of 45S5 bioglass coatings deposited by high velocity suspension flame spraying (HVSFS), J. Mater. Sci. Mater. Med. 22 (5) (2011) 1303–1319, https://doi.org/10.1007/s10856-011-4307-6.

[26] D. Bellucci, et al., High velocity suspension flame sprayed (HVSFS) potassium-based bioactive glass coatings with and without TiO 2 bond coat, Surf. Coatings Technol. 206 (19–20) (2012) 3857–3868, https://doi.org/10.1016/j.surfcoat.2012.02.041.

[27] G. Bolelli, et al., Microstructure and in-vitro behaviour of a novel High Velocity Suspension Flame Sprayed (HVSFS) bioactive glass coating, Surf. Coatings Technol. 205 (4) (2010) 1145–1149, https://doi.org/10.1016/j.surfcoat.2010.03.063.

[28] G. Bolelli, V. Cannillo, R. Gadow, A. Killinger, L. Lusvarghi, J. Rauch, Processing and characterisation of high-velocity suspension flame sprayed (HVSFS) bioactive glass coatings, Ceram. - Silikaty 54 (1) (2010) 1–7.

[29] "BS ISO 23317:2014 - Implants for Surgery - In Vitro Evaluation for Apatite-forming Ability of Implant Materials," p. 13, 2014.

[30] A. Cattini, D. Bellucci, A. Sola, L. Pawłowski, V. Cannillo, Microstructural design of functionally graded coatings composed of suspension plasma sprayed hydroxyapatite and bioactive glass, J. Biomed. Mater. Res. - Part B Appl. Biomater. 102 (3) (2014) 551–560, https://doi.org/10.1002/jbm.b.33034.

[31] G.W. MOREY, The constitution of glass, J. Am. Ceram. Soc. 17 (1–12) (1934) 315–328, https://doi.org/10.1111/j.1151-2916.1934.tb19332.x.

[32] D. Bellucci, G. Bolelli, V. Cannillo, A. Cattini, A. Sola, In situ Raman spectroscopy investigation of bioactive glass reactivity: simulated body fluid solution vs TRIS-buffered solution, Mater. Charact. 62 (10) (2011) 1021–1028, https://doi.org/10.1016/j.matchar.2011.07.008.

[33] V. Anand, K.J. Singh, K. Kaur, Evaluation of zinc and magnesium doped 45S5 mesoporous bioactive glass system for the growth of hydroxyl apatite layer, J. Non-Cryst. Solids 406 (2014) 88–94, https://doi.org/10.1016/j.jnoncrysol.2014.09.050.

[34] A.M.B. Silva, C.M. Queiroz, S. Agathopoulos, R.N. Correia, M.H.V. Fernandes, J. M. Oliveira, Structure of SiO 2 -MgO-Na 2 O glasses by FTIR, Raman and 29 Si MAS NMR, J. Mol. Struct. 986 (1–3) (2011) 16–21, https://doi.org/10.1016/j.molstruc.2010.11.023.

[35] V.V. Nosenko, A.M. Yaremko, V.M. Dzhagan, I.P. Vorona, Y.A. Romanyuk, I. V. Zatovsky, Nature of some features in Raman spectra of hydroxyapatite-containing materials, J. Raman Spectrosc. 47 (6) (2016) 726–730, https://doi.org/10.1002/jrs.4883.

[36] G. Penel, G. Leroy, C. Rey, E. Bres, MicroRaman spectral study of the PO4 and CO3 vibrational modes in synthetic and biological apatites, Calcif. Tissue Int. 63 (6) (1998) 475–481, https://doi.org/10.1007/s002239900561.

[37] S. N. Kane, A. Mishra, and A. K. Dutta, "Preface: international conference on recent trends in physics (ICRTP 2016)," J. Phys. Conf. Ser., vol. 755, no. 1, 2016, doi: https://doi.org/10.1088/1742-6596/755/1/011001.

[38] G. Bolelli, J. Rauch, V. Cannillo and R L. Lusvarghi, "Investigation of high-velocity suspension flame sprayed (HVSFS) glass coatings," Mater. Lett., vol. 62, pp. 2772–2775, 2008, doi: https://doi.org/10.1016/j.matlet.2008.01.049.

[39] R.W. Trice, K.T. Faber, Role of lamellae morphology on the microstructural development and mechanical properties of small-particle plasma-sprayed alumina, J. Am. Ceram. Soc. 83 (4) (2000) 889–896, https://doi.org/10.1111/j.1151-2916.2000.tb01290.x.

[40] Z. Pala, E. Shaw, J.W. Murray, N. Senin, T. Hussain, Suspension high velocity oxy-fuel spraying of TiO2: a quantitative approach to phase composition, J. Eur. Ceram. Soc. 37 (2) (2017) 801–810, https://doi.org/10.1016/j.jeurceramsoc.2016.08.030.

[41] M. Bai, R. Khammas, L. Guan, J.W. Murray, T. Hussain, Suspension high velocity oxy-fuel spraying of a rutile TiO2 feedstock: microstructure, phase evolution and photocatalytic behaviour, Ceram. Int. 43 (17) (2017) 15288–15295, https://doi.org/10.1016/j.ceramint.2017.08.068.

[42] P. Ctibor, M. Hrabovský, Plasma sprayed TiO2: the influence of power of an electric supply on particle parameters in the flight and character of sprayed coating, J. Eur. Ceram. Soc. 30 (15) (2010) 3131–3136, https://doi.org/10.1016/j.jeurceramsoc.2010.05.029.

[43] A. Cattini, et al., Suspension plasma sprayed bioactive glass coatings: effects of processing on microstructure, mechanical properties and in-vitro behaviour, Surf. Coatings Technol. 220 (2013) 52–59, https://doi.org/10.1016/j.surfcoat.2012.10.076.

[44] Y. Yu, Z. Bacsik, and M. Edén, "Contrasting in vitro apatite growth from bioactive glass surfaces with that of spontaneous precipitation," Materials (Basel)., vol. 11, no. 9, p. 1690, 2018, doi: https://doi.org/10.3390/ma11091690.

[45] C.V. Brovarone, E. Verné, P. Appendino, Macroporous bioactive glass-ceramic scaffolds for tissue engineering, J. Mater. Sci. Mater. Med. 17 (11) (2006) 1069–1078, https://doi.org/10.1007/s10856-006-0533-8.
[46] K. Franks, V. Salih, J.C. Knowles, I. Olsen, The effect of MgO on the solubility behavior and cell proliferation in a quaternary soluble phosphate based glass system, J. Mater. Sci. Mater. Med. 13 (6) (2002) 549–556, https://doi.org/10.1023/A:1015122709576.
[47] L.L. Hench, Bioceramics: from concept to clinic, J. Am. Ceram. Soc. 74 (7) (1991) 1487–1510, https://doi.org/10.1111/j.1151-2916.1991.tb07132.x.
[48] T. Yabutsuka, R. Karashima, S. Takai, and T. Yao, "Effect of doubled sandblasting process and basic simulated body fluid treatment on fabrication of bioactive stainless steels," Materials (Basel)., vol. 11, no. 8, p. 1334, 2018, doi: https://doi.org/10.3390/ma11081334.
[49] A. Itl, et al., Characterization of microrough bioactive glass surface surface: surface reactions and osteoblast responses in vitro, J. Biomed. Mater. Res. 62 (3) (2002) 404–411, https://doi.org/10.1002/jbm.10273.
[50] B.D. Bovan, T.W. Thomas, D. Hummert, Z. Schwartz, Role of material surfaces in regulating bone and cartilage cell response, Biomaterials 17 (2) (1996) 137–146, https://doi.org/10.1016/0142-9612(96)85758-9.
[51] A. Saboori, M. Rabiee, F. Moztarzadeh, M. Sheikhi, M. Tahriri, M. Karimi, Synthesis, characterization and in vitro bioactivity of sol-gel-derived SiO2–CaO–P2O5–MgO bioglass, Mater. Sci. Eng. C 29 (1) (2008) 335–340, https://doi.org/10.1016/j.msec.2008.07.004.